Vibronic effect and influence of aggregation on the photophysics of graphene quantum dots

Thomas Liu, Claire Tonnelé, Shen Zhao, Loïc Rondin, Christine Elias, Daniel Medina-Lopez, Hanako Okuno, Akimitsu Narita, Yannick Chassagneux, Christophe Voisin, et al.

▶ **To cite this version:**

Thomas Liu, Claire Tonnelé, Shen Zhao, Loïc Rondin, Christine Elias, et al.. Vibronic effect and influence of aggregation on the photophysics of graphene quantum dots. Nanoscale, 2022, 10.1039/D1NR08279E . hal-03548812

HAL Id: hal-03548812
https://hal.science/hal-03548812

Submitted on 31 Jan 2022

HAL is a multi-disciplinary open access archive for the deposit and dissemination of scientific research documents, whether they are published or not. The documents may come from teaching and research institutions in France or abroad, or from public or private research centers.

L'archive ouverte pluridisciplinaire **HAL**, est destinée au dépôt et à la diffusion de documents scientifiques de niveau recherche, publiés ou non, émanant des établissements d'enseignement et de recherche français ou étrangers, des laboratoires publics ou privés.

Journal Name

ARTICLE TYPE

Cite this: DOI: 00.0000/xxxxxxxxxx

Vibronic effect and influence of aggregation on the photophysics of graphene quantum dots†

Thomas Liu,[a,*] Claire Tonnelé,[b,*] Shen Zhao,[a,+] Loic Rondin,[a] Christine Elias,[a] Daniel Medina-Lopez,[c] Hanako Okuno,[d] Akimitsu Narita,[e] Yannick Chassagneux,[f] Christophe Voisin,[f] Stéphane Campidelli,[c] David Beljonne,[b] and Jean Sébastien Lauret[a]

Received Date
Accepted Date

DOI: 00.0000/xxxxxxxxxx

Graphene quantum dots, atomically precise nanopieces of graphene, are promising nanoobjects with potential applications in various domains such as photovoltaics, quantum light emitters or bio-imaging. Despite their interesting prospects, precise reports on their photophysical properties remain scarce. Here, we report on a study of the photophysics of $C_{96}H_{24}(C_{12}H_{25})$ graphene quantum dots. A combination of optical studies down to the single molecule level with advanced molecular modeling demonstrates the importance of the coupling to vibrations in the emission process. Optical fingerprints for H-like aggregates are identified. Our combined experimental-theoretical investigations provide a comprehensive description of the light absorption and emission properties of nanographenes, which not only represents an essentiel step towards precise control of sample production, but also paves the way for new exciting physics focused on twisted graphenoid.

Introduction

Graphene quantum dots (GQDs), result of the confinement of two-dimensional graphene to a quasi-0D nanostructure, have recently attracted attention for their various promising properties [1–3] and applications including optical-gain medium [4], photovoltaics [5] or bio-imaging [6]. A widely-used route for producing graphene quantum dots is top-down chemistry. Most of the time, these techniques are based on an acid treatment of a graphitic source. It produces suspensions of small pieces of graphene with various uncontrolled shapes, sizes and chemical nature of the edges. As a consequence, their emission properties are dominated by defects states which prevent any study of the properties-structure relationship. [7,8] On the contrary, bottom-up synthesis, where graphene quantum dots are constructed from carefully selected building blocks, allows the production of topologically precise graphenoid nanostructures, where symmetries, size and edges can be perfectly controlled [9–11]. This opened up the way for the specific tailoring of nanostructures according to desired applications, including charge transport [12] or spin properties [13]. Similarly, the energy gap tunability provides a perspective for the control of GQDs' photophysical properties, and the achievement of tunable light sources [14]. Nevertheless, accessing these exciting properties toward the development of devices requires advanced basic studies. Despite the extensive research activities to develop their synthesis, in-depth studies of photophysical properties of GQDs remain scarce. [15] First, the investigation of GQDs' photophysical properties generally focuses solely on measurements in solution. [16,17] Moreover, extensive theoretical studies on GQDs rarely take vibrational aspects into consideration. [18,19] However, the vibronic coupling is mentioned as a possible reason explaining the brightening of some dark states, without being formally addressed in the calculations. [20] In this paper, we report on a comprehensive study of the fluorescence of GQDs by the combination of several experimental techniques, including single object spectroscopy, and molecular modeling. Here, we focus on $C_{96}H_{24}(C_{12}H_{25})_6$ GQDs (called $C_{96}C_{12}$ hereafter), that are composed of a C_{96} graphenoid core, with $C_{12}H_{25}$ alkyl sidechains placed in periphery to enhance solubility (Figure 1(a). We first focus on the spectroscopy of GQD monomers. Then, the effect of aggregation on the optical transitions is investigated, bringing a new light on fluorescence spectrum of ensemble of GQDs.

* both authors have the same contribution.
[a] Université Paris-Saclay, ENS Paris-Saclay, CentraleSupélec, CNRS, LuMIn, Orsay, France; E-mail: lauret@ens-paris-saclay.fr
[b] CMN, Université MONS, Belgium.
[c] Université Paris-Saclay, CEA, CNRS, NIMBE, LICSEN, 91191, Gif-sur-Yvette, France.
[d] University Grenoble Alpes, CEA INAC-MEM, F-38000 Grenoble, France.
[e] Max Planck Institute for Polymer Research, Ackermannweg 10, 55128 Mainz, Germany.
[f] LPENS, PSL, CNRS, Université de Paris, Sorbonne Université, 75005 Paris, France.
[+] Current address: Fakultät für Physik, Munich Quantum Center, and Center for NanoScience (CeNS), Ludwig-Maximilians-Universität München, Geschwister-Scholl-Platz 1, 80539 München, Germany.
† Electronic Supplementary Information (ESI) available: See DOI: 10.1039/b000000x/

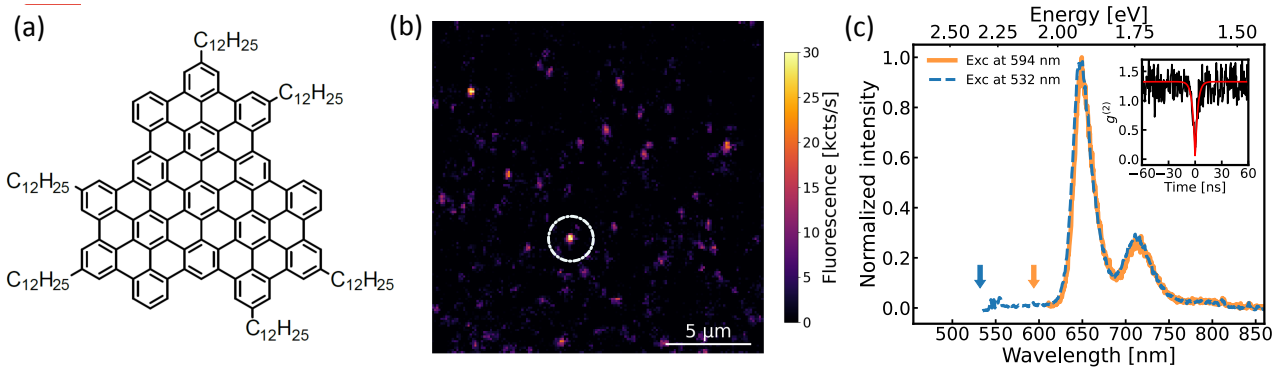

Fig. 1 (a) Chemical formula of the $C_{96}C_{12}$ graphene quantum dot (GQD). (b) Fluorescence raster scan of the GQD sample recorded with the confocal microscope. The false color represents the fluorescence intensity in kilo counts per second. The dotted white circle highlights a particular spot which spectrum is displayed on Figure 1(c). (c) PL spectra of a single GQD when excited at 594 nm (in orange) and 532 nm (in blue dashed line). Color arrows indicate the respective excitation wavelengths. Inset: second-order correlation function $g^{(2)}$ with single-emitter signature ($g^{(2)}(0) < 0.5$).

Experimental

Synthesis

The details of the synthesis have already been reported[14,21]. Briefly, $C_{96}C_{12}$ GQD is synthesized in two steps from the 1,3,5-triethynylbenzene and 2,5-diphenyl-3,4-di(4-dodecylphenyl)-cyclopentadien-1-one, similarly to litterature procedure,[22] via Diels-Alder cycloaddition followed by oxidative cyclodehydrogenation in the presence of $FeCl_3$. The intermediate compounds are fully characterized and the GQDs' complete dehydrogenation is checked by MALDI-TOF mass spectrometry (see Supplementary Figures S9 and S10).

Sample preparation

Stock solutions of GQD dispersion with a target concentration of $3 \times 10^{-5}\,\mathrm{mol \cdot L^{-1}}$ were obtained by dispersing GQDs powder in 1,2,4-trichlorobenzene (TCB) by stirring for 24 h at room temperature after sonicating the solution for a few seconds (Elma, Elmasonic P). Absorption measurements were directly performed on stock solutions. Stock solutions were then diluted by 100 for fluorescence measurements in solution. In order to prevent any oxygen photo-assisted degradation, the samples are stored in a glovebox under inert atmosphere (Ar). Samples for single-molecule experiments were obtained by mixing one volume of the diluted GQD solution with one volume of a solution of polystyrene in TCB (at 10 % in wt). The solution was spin-coated on a glass coverslip for 180 s at 2000 rpm. Before the spin-coating procedure, the glass coverslip was subjected to 5 minutes of plasma cleaner. The sample was annealed on a hotplate at 90 °C for 1 h.

Optical measurements

Absorption spectroscopy was performed using a commercial spectrometer (PerkinElmer Lambda 950) with 2 mm optical path cuvettes (Hellma Analytics, Quartz Glass High Performance cuvette). Solution PL and PLE measurements were performed using a commercial spectrofluorometer (Horiba, FluoroMax+), with 10 mm optical path cuvette. Single-molecule measurements were performed using a home-built confocal microscope under ambient conditions. The excitation sources were a continuous-wave diode laser at 594 nm (Cobolt Mambo 100) and a continuous-wave solid-state laser at 532 nm (Sapphire Coherent). The excitation beam was focused onto the sample using an oil-immersion microscope objective (NA=1.42, Olympus PLAPON 60XO) mounted on a piezoelectric XYZ scanner (Mad City Labs Inc.). Luminescence from the sample was collected in reflection using the same objective, with the excitation beam filtered by a dichroic mirror (zt 594 RDC, Chroma and 552 edge LaserMux, Semrock) and long-pass filters (FELH0600, Thorlabs or 532 EdgeBasic, Semrock), and then directed into a spectrometer (SP-2358, Princeton Instruments) coupled with a LN-cooled CCD camera (PyLoN:100BR eXcelon, Princeton Instruments) or into two silicon-based avalanche photodiodes (SPCM-AQR-13, PerkinElmer) mounted in a Hanburry Brown and Twiss configuration. Second-order photon correlation measurements were done using a time-correlated single-photon counting module (PicoHarp300, PicoQuant). A supercontinuum pulsed laser (Fianium), tuned at 580 nm using an acousto-optic tunable filter, was used for lifetime measurements, with 6 ps pulse width and 60 MHz repetition rate.

Computational details

$C_{96}C_{12}$ GQD electronic structure and optical properties have been computed in the gas phase within the framework of the density functional theory (DFT) and time-dependent DFT (TDDFT) using the Gaussian 16 package[23]. The molecular geometry was optimized at the B3LYP/6-31G(d) level. On the basis of this equilibrium structure, the dependence of the excitation energies has been explored for B3LYP, HSE06, M06-2X, ωB97X-D, and LC-ωPBE (ω=0.110 $\mathrm{Bohr^{-1}}$) exchange-correlation functionals (XCF), and the latter selected for all TDDFT calculations reported below (see Supplementary Table S2). Molecular dynamics (MD) simulations were carried out to investigate dynamical behavior of GQD monomers and dimers in the 1,2,4-TCB solvent (same as experiments reported here) using the NAMD code[24]. All simulations started from a low-density box with 150 Å side and were first equilibrated for 2 ns in the NpT isothermal-isobaric ensemble with N the number of particles, $p = 1000$ atm and

$T = 298.15$ K, applying periodic boundary conditions in all three dimensions. In the case of the monomer, the system was further equilibrated for 5 ns at $p = 1$ atm before a 5 ns production run. For the dimer, an equilibration of 55 ns was performed prior to a 10 ns production run. A time step of 1 fs was used, controlling temperature by rescaling velocities every 100 steps, and pressure with a weak-coupling thermostat. A cutoff radius of 12 Å was employed to truncate the short-range nonbonded interactions, while long-range electrostatic interactions were evaluated through the particle-mesh Ewald method[25]. GQD and solvent molecules were modeled using the General AMBER Force Field[26] (GAFF), with electrostatic potential-fitted partial atomic charges derived from DFT calculations at the B3LYP/6-31G(d) level. To assess the impact of structural dynamics on the optical properties of $C_{96}C_{12}$ GQD monomer and dimer, TDDFT calculations were performed on 43 and 7 frames extracted from MD simulations, respectively.

Results and Discussion

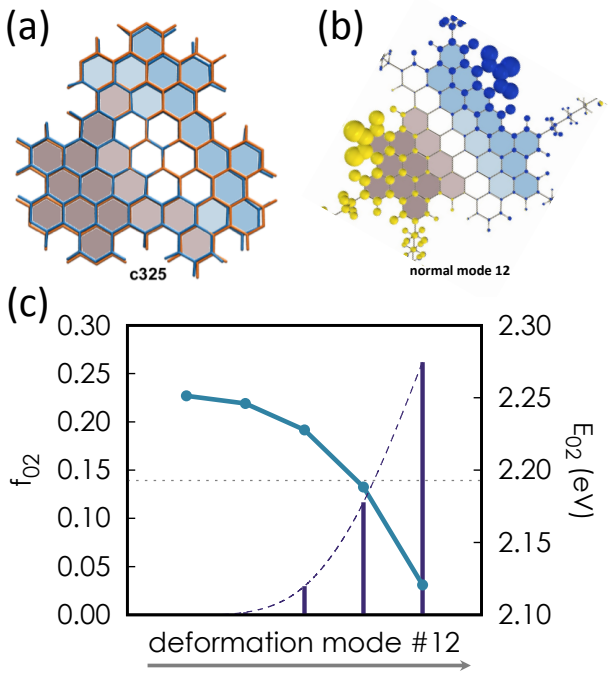

Fig. 2 (a) Deformation patterns for the structure extracted from frame c325 of the molecular dynamics simulations. Colored rings correspond to out-of-plane deformations, upward (dark-grey-filled) or downward (blue-filled) relative to the molecular median plane. (b) Normal mode 12 corresponding to the deformation. (c) Evolution of the oscillator strength and excitation energy for the $S_0 \rightarrow S_2$ transition along the normal mode deformation.

As we have recently demonstrated, $C_{96}C_{12}$ photoluminescence can be addressed at the single object level[14]. This is a critical advantage to probe the intrinsic photophysical properties of these objects. We thus first investigate the photoluminescence properties of isolated single GQD dispersed in a polystyrene matrix. To identify single GQDs, we first measure the second-order correlation function of photon emission ($g^{(2)}(\tau)$), integrated over the whole spectrum, on a diffraction-limited spot (see Figure 1(b)). The appropriate antibunching signature ($g^{(2)}(0) < 0.5$, inset of Figure 1(c)) ensures that a single GQD is addressed. We then measure on such single GQDs, the emission spectrum, under a $\lambda = 594$ nm excitation. The orange curve in Figure 1(c) displays a typical PL spectrum. The characteristic emission lines of GQD monomer with the main emission peak around 650 nm are detected. This matches our previous report[14]. The presence of defects in GQDs synthesized by top-down methods results in a fluorescence spectrum that depends on the excitation wavelength[8]. Therefore, to test the presence of higher energy emission lines, we increase the excitation energy (decrease the excitation wavelength to $\lambda = 532$ nm), and record a spectrum on the very same GQD. As shown in Figure 1(c), the emission spectrum is not impacted by the excitation wavelength. This observation confirms that the photon emission from this single object results from intrinsic electronic transitions of GQDs, and not from a collection of defect states characterized by a wide range of transition energy. In order to get deeper insight into the photophysics, DFT/TDDFT calculations have been performed. The four first excited states of $C_{96}C_{12}$ GQD monomer can be described as combinations of excitations involving doubly degenerate delocalized HOMO and LUMO of e" symmetry (see Figure S3 for the description of the orbitals). It results in two low-lying dark states (S_1, S_2) and two degenerate bright states (S_3, S_4) at higher energy (see Supplementary Table S3). Interestingly, transitions to S_1 and S_2 are forbidden by symmetry. It highlights the importance of the shape of GQDs to tailor their properties. The GQD studied here have a C_3 symmetry. A similar behaviour has been reported theoretically for GQDs with D_{6h} symmetry, where a breaking of the symmetry leads to a brightening of the two low-energy dark states.[20] More specifically, for the $C_{96}C_{12}$, S_1 and S_3 correspond to antisymmetric and symmetric linear combinations of HOMO-1 $\rightarrow$ LUMO and HOMO $\rightarrow$ LUMO+1 excitations, respectively, while S_2 and S_4 involve symmetric and antisymmetric combinations of HOMO-1 $\rightarrow$ LUMO+1 and HOMO $\rightarrow$ LUMO, respectively. According to Clar's notation for fully benzenoid polycyclic aromatic hydrocarbon (PAHs) like $C_{96}C_{12}$ GQDs, these states can be associated to the α-, p-, and β-bands, in the order of increasing energy.[11] Accounting for dynamical behavior of the system, an average transition energy of 2.55 eV is computed for the bright states (see Supplementary Table S4). This result fits well with the transition at 478 nm (2.59 eV) measured in optical absorption spectroscopy (see Figure 4(a) and Supplementary Figure S6). As mentioned above, the two first singlet states are dark by symmetry. Nevertheless, several processes can be at the origin of a symmetry breaking as it has been observed in many systems.[27–30] In particular, the calculations leading to the forbidden transitions were performed on the planar geometry of the GQD. Interestingly, the transition towards S_2 appears to be partially allowed when the molecular dynamics at room temperature is included in the calculations. Indeed, it gives a non-zero oscillator strength $f > 0.1$, indicating coupling of the singlet states to vibrational modes. In particular, low frequency modes that can be associated to the out-of-plane distortion of the nanographene core turn-on the $S_0 \rightarrow S_2$ transition. For the sake of illustration, Figure 2(a), (b) respectively show a frame obtained in molecular dynamics simulations

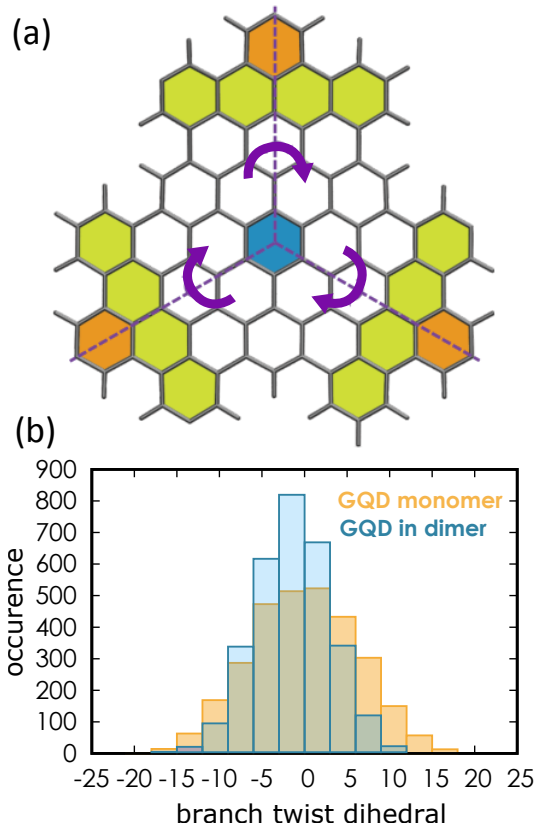

Fig. 3 (a) Out-of plane distortion of the GQDs (b) Distributions of the branch twist dihedral angle of the GQD branches with respect to the median plane: for a monomer (yellow) and for a GQD in a dimer (blue).

and the corresponding calculated normal mode. Following the deformation of this mode, the oscillator strength increases and finally exceeds 0.2 (Figure 2(c)). Surprisingly, and in disagreement to what was expected[20], we note that such an intensity borrowing effect does not occur for the $S_0 \rightarrow S_1$ transition that is characterized by vanishing transition densities on all sites, whether the molecule is distorted or not (see Supplementary Figure S5). Figure 2(c) shows that the excitation energy of the $S_0 \rightarrow S_2$ transition decreases with increasing deformation amplitude of the considered mode. We therefore speculate that either this transition becomes the lowest-lying singlet excited state upon molecular distortion, state from which the emission occurs, or that $S_0 \rightarrow S_1$ remains the lowest-lying singlet excited state but, being dark, is not observed experimentally. However, the relatively high fluorescence quantum yield of the $C_{96}C_{12}$ ($\geq$ 35%)[14] does not tally with such a dark state at lower energy than the emissive state, hence we believe the first scenario to be more likely. We note that the lines at lower energies in Figure 1(c) correspond to vibronic replicas with a quantum of vibration of $\sim$ 170 meV which is close to the C=C stretching mode energy.

Despite their high interest, one major hurdle of GQDs that slows down basic studies as well as their use in devices is their tendency to aggregate through π-π interaction due to the large size of their sp^2 carbon core. This problem appears clearly while looking at the objects present in the solution. For example, transmission electron microscopy (TEM) reveals lots of small particles (<2 nm), corresponding to individual monomers or few stacked GQDs dispersed on the graphene support layer, as well as columns with few GQDs vertically stacked (see Supplementary Figure S11). Note that such columnar structures have been reported for the specific GQD structure we study here[9] and for other nanographene structures.[31] These observations strongly confirm the existence of H-type aggregates in the solution, with a high size dispersion. In this context, we have been looking for a spectral signature of the aggregation in the optical properties of GQDs.

In order to explore the effect of aggregation on the electronic properties, we first extended our calculations on a dimer of $C_{96}C_{12}$. Structurally, the dimer of $C_{96}C_{12}$ GQD presents an H-like configuration with an average interlayer distance of 3.48 Å, indicating $\pi - \pi$ interactions within the dimer. The most stable configuration shows a twist angle between the two GQDs of 23°±2°. Accordingly, the formation of a dimer is accompanied by a blue-shift of the optical transition by about 30 meV (see Supplementary Table S5). The average oscillator strength over the first ten low-lying states amounts to 0.004, which is two orders of magnitude lower than for the monomer. This should lead to a decrease of the fluorescence efficiency in these H-like aggregates. Moreover, we performed the same TDDFT excited-state calculations coupled to MD simulations as done for the monomer in order to probe the effect of lattice fluctuations on the electronic excitations. Compared to the monomer case, the amplitude of the geometric distortions is reduced in the physical dimer. Figure 3(a) shows the out-of plane distortion of the GQDs characterized by the branch twist dihedral angle of the GQD branches with respect to the median plane. The distributions of this dihedral angle for a GQD as a monomer and in the dimer are plotted in Figure 3(b). We observe that the distribution of angles for the monomer is broader than for the GQD in the dimer with a standard deviation of $\sigma_{mono} = 6.2°$ for the monomer versus $\sigma_{dimer} = 4.4°$ and 4.6° for the two GQDs constituting the dimer (see Supplementary Figure S4 for the results on the second GQD of the dimer). Most importantly, these structural deformations have a very small impact on the oscillator strength of the lowest-lying states. In summary, these calculations predict that the coupling between monomers in small aggregates leads to a global increase of the energy of the S_0-S_n transition and a decrease of the radiative decay rate from the emissive states.

The UV/Visible absorption spectrum of the GQD dispersed in 1,2,4-trichlorobenzene (TCB) given in Figure 4(a) shows broad features typical for large PAHs in solution[10,32]. The main absorption peak is composed of two bands at 455 nm and 475 nm. On the red side of this band, one can observe two other features at 576 nm and 635 nm. This correctly corresponds to the absorption profile previously reported for this specific GQD[9,14]. While the main features of the absorption spectrum are fully reproducible, the details of the structures can vary from one solution to another with more or less pronounced broadening (see Supplementary Figure S6). The fluorescence spectrum of GQDs in solution is displayed on Figure 4(b). It shows two strong peaks at 644 nm (peak 1) and at 703 nm (peak 2), which correctly match the emission lines we previously observed in the single-molecule

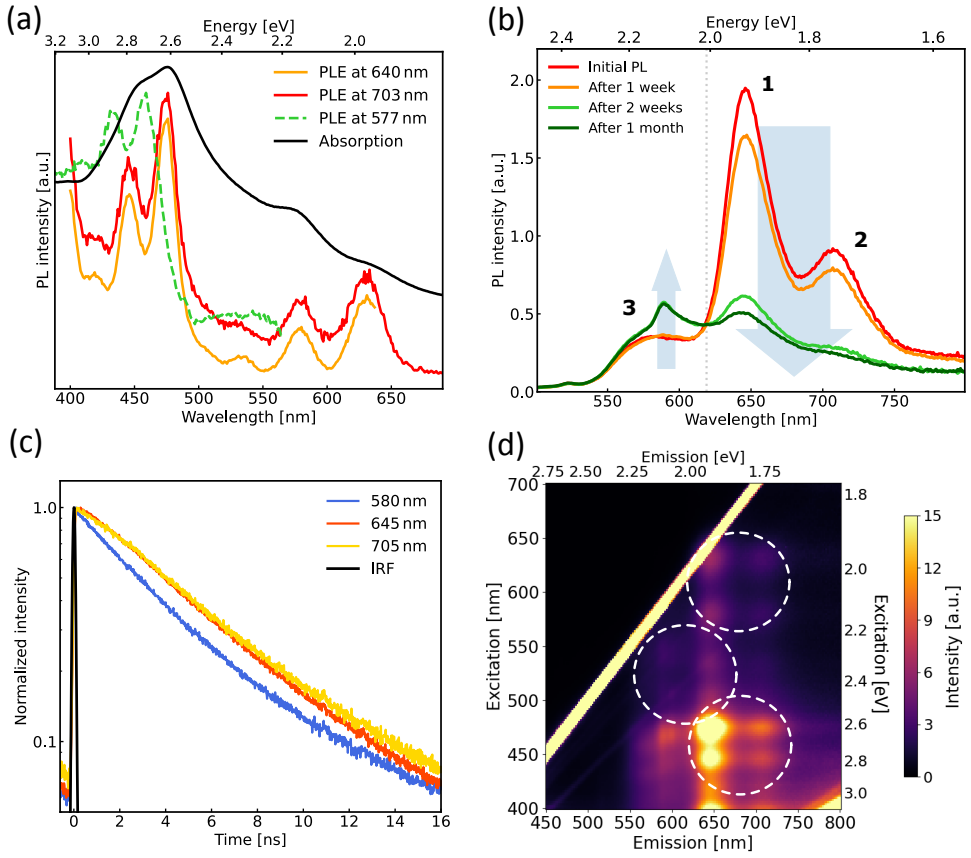

Fig. 4 (a) Absorption spectrum of the $C_{96}C_{12}$ GQD in TCB and PLE spectra collected at the wavelengths of PL peaks 1, 2 (solid lines) and 3 (dashed line). (b) Evolution over time of the fluorescence spectrum of $C_{96}C_{12}$ in TCB. (c)Time-resolved fluorescence spectra detected at the wavelengths of PL peaks 1 (red), 2 (yellow) and 3 (blue) (d) PLE 2D map of $C_{96}C_{12}$ in TCB.

measurements (see Figure 1(c)). The energy split between peaks 1 and 2 is $\sim$167 meV, also consistent with the vibronic replica observed on single-molecule spectra. An additional broader band at 577 nm, labeled peak 3, is also noticed. The origin of this higher energy emission peak is yet unclear. First, this high energy line is not detected in the single-molecule measurements reported in Figure 1(c) excluding that it arises from intrinsic fluorescence, for instance from a higher singlet state. Therefore, it can be rather related to additional fluorescent species in the solution. This interpretation is strengthened by the time-resolved PL (TR-PL) measurements performed at the wavelengths of peaks 1, 2 and 3, as plotted in Figure 4(c). The TR-PL spectra collected at 650 nm and 705 nm show the same mono-exponential decay, with a lifetime of $\sim$5 ns, in agreement with experiments on single molecules.[14] The observation of the same dynamics for the emission at the two wavelengths is a solid indication that peaks 1 and 2 in the PL result from the emission of the same object, in our case GQD monomers. The dynamics observed at 575 nm shows a multi-exponential decay, with an average shorter fluorescence lifetime. This stark difference in the dynamics confirms that the emission from peak 3 stems from different fluorescent objects. As a first hypothesis, synthesis by-products could be considered as a possible origin for this peak. Few impurities, with masses close to the one of $C_{96}C_{12}$, are detected in MALDI-TOF experiments. The different possible structures corresponding to the detected mass are discussed in the supplementary information. Nevertheless, Figure S6 shows that the intensity ratio between PL lines 1 and 3 varies from one suspension to another inside the same batch of GQDs. Making the assumption that the intensities of the PL lines are proportional to the concentrations, this observation demonstrates that the amount of each species varies from one suspension to another, which is unlikely if line 3 would originate only from synthesis by-products. To get more specific insights on the evolution of the fluorescent species population in the solution we follow its PL time evolution. Figure 4(b) gives an example of the evolution of the PL spectrum after leaving the sample in an inert Ar environment. We observe that the intensity of peaks 1 and 2 associated to the emission of GQD monomers shows a net decrease while the intensity of peak 3 at higher energy increases. In this particular case, an iso-emissive point is observed at 615 nm (see Figure S7 for other examples). The presence of an iso-emissive point is the signature of a population conversion between the GQDs monomers (peaks 1 and 2) and a molecular species emitting at higher energy (peak 3). This again excludes that line 3 arises only from synthesis by-products. Finally, while the intensity of the fluorescence lines of GQD monomers is reduced by approximately a factor four, the intensity of peak 3 is increased only by a factor $\sim$ 1.5. It demonstrates that the species

in which the GQDs monomers are converted into possess a lower fluorescence quantum yield. This is in line with the decrease of oscillator strength predicted by the calculations. Moreover, the decrease of fluorescence upon aggregation is also commonly observed in other types of chromophores. This is for instance one limitations of the efficiency of organic light-emitting diodes.[33] In summary, peak 3 is blue-shifted in comparison to the lines of GQDs monomers with a lower quantum yield. Therefore, in line with the theoretical predictions, this line can be related, at least partially, to the emission of small aggregates of $C_{96}C_{12}$ (dimers, trimers...).

Our theoretical calculations indicate that the first four transition should be blue-shifted upon aggregation. Therefore we performed PL excitation (PLE) spectroscopy. First, PLE 2D map is plotted in Figure 4(d). Some hot spots are observed that are related to resonances between excited and emissive states. In particular one can observe the intense spots related to the emission of monomers when excited on the $S_{3,4}$ transitions. Moreover, this 2D map highlights some periodic structures marked by the white dotted circles in the figure. These periodic features are characteristic of the Frank-Condon progression of vibronic replicas. To go into more details, we focus on PLE traces detected at several emission wavelengths as displayed in Figure 4(a). The PLE spectra recorded at 640 nm and at 703 nm lines (emission lines of monomers) present unambiguously the same excitation peaks, which is predictable for PLE spectra originating from the same object. From lowest to highest energy, the wavelengths of the lines are: 631 nm, 579 nm, 535 nm, 475 nm, 446 nm, 420 nm. The energy splits between the three peaks at lower energy and the three peaks at higher energy are respectively ~ 176 meV and ~ 170 meV. These values are again compatible with the C=C vibration energy. This behaviour is fully reproducible from one sample to another. Let us now focus on the high energy emission line 3 at 577 nm. One can see that the excitation energy resonances related to line 3 are blue-shifted by $\sim$ 100 meV. The blue-shift of the transition, that is fully reproducible, strongly supports the interpretation that line 3 includes a contribution from the emission of small aggregates of $C_{96}C_{12}$ GQDs. Calculations appear to underestimate the blue-shift due to aggregation (30 meV vs 100 meV). This is possibly related to the presence of larger aggregates in the sample than the simple dimers considered in the calculations. Moreover, on this particular sample, the periodic structures in PLE spectra are also observed on the emission line 3. From lowest to highest energy, the wavelengths of the lines are: 458 nm, 433 nm, 411 nm. The energy split between these lines are 153 meV, which gives a value lower than for the lines observed for GQDs monomers. This lower value in comparison with the monomer would reflect a decrease of the C=C energy mode in the aggregate. Finally, as for the absorption spectra, the fine structure of the PLE spectra is varying on all measured samples. Indeed, for the same powder of GQDs, depending on the suspension process, the blue-shifted PLE spectra show more or less pronounced vibronic progression. The energy shift of the electronic levels, the lowering of the vibration mode and the broadening of the lines originate from the interactions between the monomers inside an aggregate. This interaction is therefore depending on the details of the structure of the aggregate. Thus, the TEM investigations mentioned previously show that the sample contains aggregates in a H-like configuration with different structures going from two to dozen of layers, and with different degrees of disorder. The amount of each type of aggregate depending on the solubilization process, this can explain the differences observed from one suspension to another.

Conclusions

In summary, we investigated the photophysics of the $C_{96}C_{12}$ GQDs both at the single-molecule level and in suspension. We demonstrated that the emission spectrum of single GQDs does not depend on the excitation wavelength and arises from intrinsic quantum states. Moreover, calculations showed that the vibrations of the molecule core brightens the second singlet transition while letting the first one dark. The highlight of the importance of the electron-vibration coupling in the emission process suggests digging into this question more deeply. In particular, single-molecule experiments at low temperature are on-going. The reduction of the linewidth will enable precise insight into the vibronic coupling in GQDs. Moreover, our results suggest also that investigating GQDs with other symmetries, such as D_{2h},[20] but with the same number of atoms would be very helpful for understanding the structure-properties relationship.Finally, we explored the effect of aggregation on the optical transitions of GQDs. We showed, both theoretically and experimentally, that it leads to a blue shift of the transition and to a decrease of the quantum yield. Beyond the better understanding of the photophysics of GQDs, this work opens the way for extensive studies focused on the physics of small aggregates of GQDs, that can be viewed as twisted graphenoids.

Authors contribution

TL, CE and SZ have performed the optical expriments. CT have performed the calculations and simulations. DM and SC have synthesized and characterized the GQDs. HO have performed the TEM measurements. LR, DB and JSL have supervised the work and written the paper. All the authors participated to the interpretations of the data. TL and CT have equal contribution.

Acknowledgements

This work has been financially supported by the FLAG-ERA Grant OPERA by DFG 437130745 and ANR-19-GRF1-0002-01, by the ANR-DFG NLE Grant GRANAO by DFG 431450789 and ANR-19-CE09-0031-01, by a public grant overseen by the French National Research Agency (ANR) as part of the "Investissements d'Avenir" program (Labex NanoSaclay, reference: ANR-10-LABX-0035). Computational resources have been provided by the Consortium des Équipements de Calcul Intensif (CÉCI), funded by the Fonds de la Recherche Scientifiques de Belgique (F.R.S.-FNRS) under Grant No. 2.5020.11, as well as the Tier-1 supercomputer of the Fédération Wallonie-Bruxelles, infrastructure funded by the Walloon Region under the grant agreement n1117545. D.B. is a FNRS Research Director.

Notes and references

1 K. Müllen, *ACS Nano*, 2014, **8**, 6531–6541.

2 J. Wu, W. Pisula and K. Müllen, *Chemical Reviews*, 2007, **107**, 718–747.

3 A. Xu, G. Wang, Y. Li, H. Dong, S. Yang, P. He and G. Ding, *Small*, 2020, **16**, 2004621.

4 G. M. Paternò, Q. Chen, X. Y. Wang, J. Liu, S. G. Motti, A. Petrozza, X. Feng, G. Lanzani, K. Müllen, A. Narita and F. Scotognella, *Angewandte Chemie - International Edition*, 2017, **56**, 6753–6757.

5 X. Yan, X. Cui, B. Li and L. S. Li, *Nano Letters*, 2010, **10**, 1869–1873.

6 M. R. Younis, G. He, J. Lin and P. Huang, *Frontiers in Chemistry*, 2020, **8**, 1–25.

7 L. Li, G. Wu, G. Yang, J. Peng, J. Zhao and J. J. Zhu, *Nanoscale*, 2013, **5**, 4015–4039.

8 Q. Xu, Q. Zhou, Z. Hua, Q. Xue, C. Zhang, X. Wang, D. Pan and M. Xiao, *ACS Nano*, 2013, **7**, 10654–10661.

9 Ž. Tomović, M. D. Watson and K. Müllen, *Angewandte Chemie - International Edition*, 2004, **43**, 755–758.

10 X. Yan, X. Cui and L. S. Li, *Journal of the American Chemical Society*, 2010, **132**, 5944–5945.

11 R. Rieger and K. Müllen, *Journal of Physical Organic Chemistry*, 2010, **23**, 315–325.

12 M. Imran, C. M. Wehrmann and M. S. Chen, *Journal of the American Chemical Society*, 2020, **142**, 38–43.

13 F. Lombardi, A. Lodi, J. Ma, J. Liu, M. Slota, A. Narita, W. K. Myers, K. Müllen, X. Feng and L. Bogani, *Science*, 2019, **366**, 1107–1110.

14 S. Zhao, J. Lavie, L. Rondin, L. Orcin-Chaix, C. Diederichs, P. Roussignol, Y. Chassagneux, C. Voisin, K. Müllen, A. Narita, S. Campidelli and J.-S. Lauret, *Nature Communications*, 2018, **9**, 3470.

15 M. Semeniuk, Z. Yi, V. Poursorkhabi, J. Tjong, S. Jaffer, Z.-H. Lu and M. Sain, *ACS Nano*, 2019, **13**, 6224–6255.

16 M. L. Mueller, X. Yan, J. A. McGuire and L.-s. Li, *Nano Letters*, 2010, **10**, 2679–2682.

17 S. Zhu, L. Wang, B. Li, Y. Song, X. Zhao, G. Zhang, S. Zhang, S. Lu, J. Zhang, H. Wang, H. Sun and B. Yang, *Carbon*, 2014, **77**, 462–472.

18 H. Riesen, C. Wiebeler and S. Schumacher, *The Journal of Physical Chemistry A*, 2014, **118**, 5189–5195.

19 Y. Li, H. Shu, S. Wang and J. Wang, *Journal of Physical Chemistry C*, 2015, **119**, 4983–4989.

20 C. Cocchi, D. Prezzi, A. Ruini, M. J. Caldas and E. Molinari, *Journal of Physical Chemistry A*, 2014, **118**, 6507–6513.

21 V. S. Iyer, M. Wehmeier, J. D. Brand, M. A. Keegstra and K. Müllen, *Angewandte Chemie International Edition in English*, 1997, **36**, 1604–1607.

22 M. Wehmeier, M. Wagner and K. Müllen, *Chemistry*, 2001, **7**, 2197–2205.

23 M. J. Frisch, G. W. Trucks, H. B. Schlegel, G. E. Scuseria, M. A. Robb, J. R. Cheeseman, G. Scalmani, V. Barone, G. A. Petersson, H. Nakatsuji, X. Li, M. Caricato, A. V. Marenich, J. Bloino, B. G. Janesko, R. Gomperts, B. Mennucci, H. P. Hratchian, J. V. Ortiz, A. F. Izmaylov, J. L. Sonnenberg, D. Williams-Young, F. Ding, F. Lipparini, F. Egidi, J. Goings, B. Peng, A. Petrone, T. Henderson, D. Ranasinghe, V. G. Zakrzewski, J. Gao, N. Rega, G. Zheng, W. Liang, M. Hada, M. Ehara, K. Toyota, R. Fukuda, J. Hasegawa, M. Ishida, T. Nakajima, Y. Honda, O. Kitao, H. Nakai, T. Vreven, K. Throssell, J. A. Montgomery Jr., J. E. Peralta, F. Ogliaro, M. J. Bearpark, J. J. Heyd, E. N. Brothers, K. N. Kudin, V. N. Staroverov, T. A. Keith, R. Kobayashi, J. Normand, K. Raghavachari, A. P. Rendell, J. C. Burant, S. S. Iyengar, J. Tomasi, M. Cossi, J. M. Millam, M. Klene, C. Adamo, R. Cammi, J. W. Ochterski, R. L. Martin, K. Morokuma, O. Farkas, J. B. Foresman and D. J. Fox, *Gaussian 16, Revision B.01.*, 2016.

24 J. C. Phillips, R. Braun, W. Wang, J. Gumbart, E. Tajkhorshid, E. Villa, C. Chipot, R. D. Skeel, L. Kalé and K. Schulten, *Journal of Computational Chemistry*, 2005, **26**, 1781–1802.

25 U. Essmann, L. Perera, M. L. Berkowitz, T. Darden, H. Lee and L. G. Pedersen, *The Journal of Chemical Physics*, 1995, **103**, 8577–8593.

26 J. Wang, R. M. Wolf, J. W. Caldwell, P. A. Kollman and D. A. Case, *Journal of Computational Chemistry*, 2004, **25**, 1157–1174.

27 F. Terenziani, A. Painelli, C. Katan, M. Charlot and M. Blanchard-Desce, *Journal of the American Chemical Society*, 2006, **128**, 15742–15755.

28 F. Terenziani, C. Sissa and A. Painelli, *The Journal of Physical Chemistry B*, 2008, **112**, 5079–5087.

29 W. Verbouwe, M. Van der Auweraer, F. C. De Schryver, J. J. Piet and J. M. Warman, *Journal of the American Chemical Society*, 1998, **120**, 1319–1324.

30 B. Dereka, D. Svechkarev, A. Rosspeintner, A. Aster, M. Lunzer, R. Liska, A. M. Mohs and E. Vauthey, *Nature Communications*, 2020, **11**, 1925.

31 X. Feng, V. Marcon, W. Pisula, M. Ryan Hansen, J. Kirkpatrick, F. Grozema, D. Andrienko, K. Kremer and K. Müllen, *Nature Materials*, 2009, **8**, 12.

32 J. A. McGuire, *physica status solidi (RRL) - Rapid Research Letters*, 2016, **10**, 91–101.

33 K. Zhang, J. Liu, Y. Zhang, J. Fan, C.-K. Wang and L. Lin, *The Journal of Physical Chemistry C*, 2019, **123**, 24705–24713.